*eXPRESS Polymer Letters Vol.15, No.7 (2021) 600–611*
*Available online at www.expresspolymlett.com*
*https://doi.org/10.3144/expresspolymlett.2021.51*

# Study of electro-induced shape-memory *Eucommia ulmoides rubber* composites reinforced with conductive carbon blacks

*L. Xia, X. Liu, Q. Wang, Z. Ma, Z. Huang**

Key Laboratory of Rubber-Plastics, Ministry of Education/Shandong Provincial Key Laboratory of Rubber-Plastics, School of Polymer Science and Engineering, Qingdao University of Science and Technology, 266042 Qingdao, P. R. China

*Received 13 July 2020; accepted in revised form 25 December 2020*

**Abstract.** We designed a series of thermo- and electro-induced double-stimulus shape-memory composites comprising natural *Eucommia ulmoides rubber* (EUR) and conductive carbon blacks (CCBs). This paper discusses the mechanical, cure, thermal, and shape-memory properties of the composites. The shape-memory properties of the composites were investigated under two stimulation conditions, heat and electricity. In these composites, the crosslinked networks acted as the fixed domain, and the crystalline regions of EUR worked as the reversible domain during the shape-memory process. CCBs were embedded in the composites as a conductive component, which endowed their electrical stimulation response. These composites exhibited excellent thermal and electrical shape-memory properties. We studied the shape-memory behavior of composites under different voltage conditions during the electrical stimulation process. Due to its excellent electrical stimulation response, natural EUR can be used in intelligent and multi-response shape-memory applications.

***Keywords:*** *polymer composites, smart polymers, rubber, thermal properties*

## 1. Introduction

Shape-memory polymers (SMPs) are a new kind of smart polymer materials [1–4] that can respond to the external environment by changing their shape under appropriate stimulation conditions, such as temperature [5–8], light [9–11], electromagnetic radiation, and solvents [12, 13]. When compared with shape-memory alloys and ceramics, SMPs have the following advantages: the ability to recover large deformations, easy self-deployment abilities, and adjustable shape response temperature. These characteristics have enabled SMPs to be applied in several areas, including biomedicine, surgical suture, stents, heart valves, tissue engineering, drug release, and vision therapy [14–18].

Based on the stimulation or recovery mechanism, SMPs may be divided into thermo-, photo-, hydro-, and electromagnetic radiation-induced SMPs. Thermo-induced SMP systems usually consist of a fixed phase that determines the initial deformation and a reversible phase that determines the reversible softening and hardening of the SMPs with the change in temperature. The fixed phase in SMPs comprises networks with chemical crosslinking (covalent bonds) or physical crosslinking (hydrogen bonds, coordination covalent bonds, and molecular entanglements), and the reversible phase comprises some of the crystal structures. Of the different types of SMPs, thermo-induced ones are the most widely studied and used. However, it has been observed that it is not easy to achieve shape-memory recovery in SMPs by direct heating in several applications, such as remote control. The heat-induced shape-memory materials are also limited by environmental factors such as external heat sources [19]. Therefore, it is necessary to stimulate materials in order to achieve a shape-memory

*Corresponding author, e-mail: xialin@qust.edu.cn

effect in a convenient, remote, diverse, and controllable manner.

Electronic shape-memory polymers (ESMPs) have attracted researchers' extensive attention due to the advantages of easy operation, wide adaptability, fast response, and remote manipulation. However, since most SMPs are insulators and cannot be electrically driven directly, conductive fillers are added to form conductive networks, enabling them to be electrically driven [20, 21]. The conductive fillers added include carbon nanotubes [22–25], conductive carbon blacks (CCBs) [26, 27], conductive fibers [28], graphene, and metal fillers [19, 30, 31]. In recent years, electronic shape-memory materials have made rapid progress due to their ability to be controlled remotely and faster response. However, challenges such as high cost and the complex process of synthesis need to be addressed. Therefore, it is important to develop composite materials with low percolation value using simple, cost-effective, and efficient preparation methods.

This paper aims to prepare electro-induced shape-memory composites by introducing CCBs into *Eucommia ulmoides rubber* (EUR) matrices. Natural EUR exists in a crystalline state at room temperature; its major component is *trans*-1,4-polyisoprene, different from *cis*-1,4-polyisoprene, which is widely found in natural rubber. Natural EUR can be used in shape-memory applications by being partially cross-linked. Our group has prepared shape-memory composites using EUR as the matrix [32–34]. EUR is similar to other shape-memory materials, such as polyethylene. However, since its mechanical strength is low, it needs to be reinforced with filler. One such material that is commonly used for reinforcement is carbon fiber. However, the addition of excessive fillers is likely to affect the shape-memory properties of the EUR materials. Although there is an amount of research on shape-memory composites, most of them are difficult to consider both the mechanical properties and shape-memory properties of the materials. To date, only a few studies have focused on the preparation of electro-induced shape-memory EUR composites and their voltage-triggered shape-memory behavior. In this study, we prepared ESMPs using EUR as the matrix material with excellent mechanical properties using a simple physical method. We studied the effect of CCB content on the mechanical, thermal, and shape-memory properties of the composites and the influence of voltage on the electrical stimulation response of the composites. The novel electro-stimulated shape-memory composites could expand the application of natural EUR, especially in the areas of special sensors and actuators.

## 2. Materials and methods

### 2.1. Materials

Natural EUR was extracted in our laboratory from Eucommia leaves. CCBs (purity ≥95%) were purchased from Aladdin Co., Ltd. (Shanghai, China). Other additives were obtained from commercial sources and were used without further purification.

### 2.2. Preparation of EUR composites

EUR was dried in a vacuum oven at 30 °C for 12 h. The EUR composites were prepared on a high-temperature open mill at 90 °C for 10 min using a standard mixing sequence. The compound formulations for different EUR/CCB ratios are presented in Table 1, and the preparation of the EUR composites is shown in Figure 1.

### 2.3. Mechanical characterization of EUR composites

Dumbbell-shaped specimens were punched out from a molded sheet using an ASTM Die C. Tests were conducted according to GB/T 1040-92 and GB/T 1843-96.

### 2.4. Electrical conductivity measurement of EUR composites

The electrical conductivities of the composites were measured using a Jandel RM2 4-point probe tester (Jandel Engineering Co.).

**Table 1.** Formulations of the EUR/CCB composites.

| Chemicals [phr][a] | A | B | C | D |
|---|---|---|---|---|
| EUR | 100 | 100 | 100 | 100 |
| ZnO | 4 | 4 | 4 | 4 |
| Stearic acid (SA) | 1 | 1 | 1 | 1 |
| *N*-cyclohexyl-2-benzothiazole sulfonamide (CBS) | 1.2 | 1.2 | 1.2 | 1.2 |
| 2,6-hydroxamino-4-methyl phenol (264) | 2 | 2 | 2 | 2 |
| Tetramethylthiuramdisulfide (TMTD) | 0.3 | 0.3 | 0.3 | 0.3 |
| S | 0.4 | 0.4 | 0.4 | 0.4 |
| CCB | 10 | 20 | 30 | 40 |

[a]Parts by weight per hundred parts of rubber

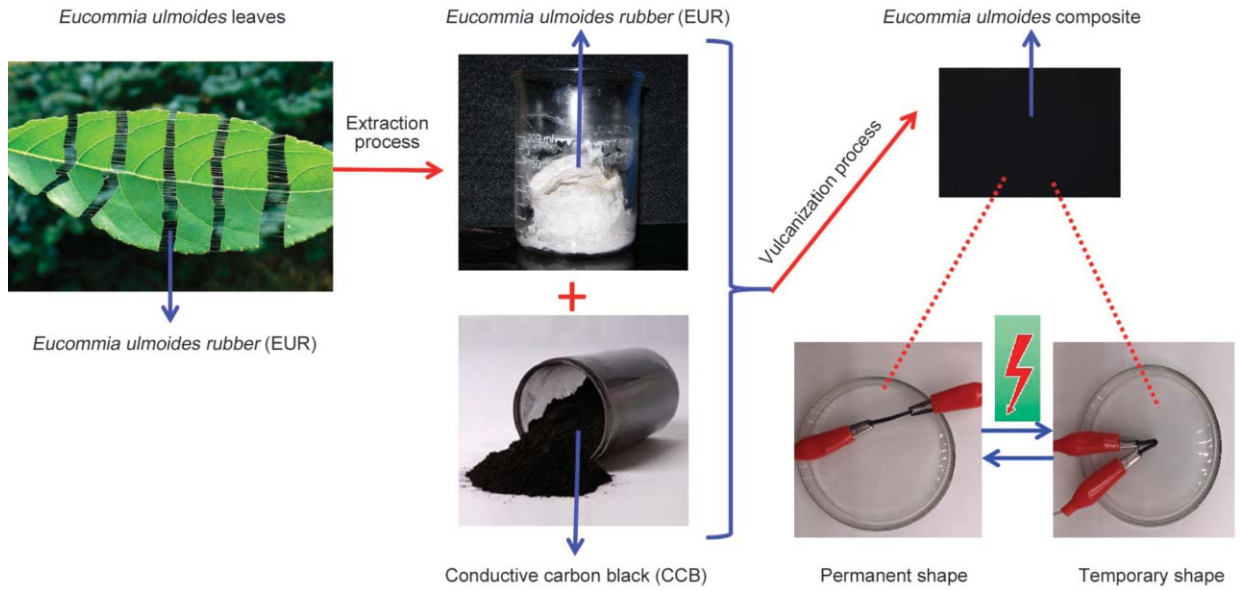


**Figure 1.** Schematic diagram of preparation of EUR/CCB composites.

### 2.5. Estimation of the crosslinking degree of EUR composites

Five samples were extracted using acetone for 12 h and dried in a vacuum oven at 80 °C until constant weight. The samples were then placed in bottles containing toluene (about 40 ml) and swelled for 72 h at 60 °C. The swollen samples were blotted using a tissue paper to remove the excess solvent, and were weighed immediately. Finally, the samples were put in a vacuum oven at 80 °C, until dry. The crosslink density of the samples was calculated according to the Equations (1) and (2):

$$-\left[\ln(1-\varphi_r)+\varphi_r+\chi\varphi_r^2\right]=V_0 n\left(\varphi_r^{1/3}-\frac{\varphi_r}{2}\right) \quad (1)$$

$$\varphi_r=\frac{m_2\rho_1}{m_2\rho_1+m_2\rho_2-m_1\rho 2} \quad (2)$$

where $m_1$ and $m_2$ are the masses of the swollen sample before and after drying, respectively; $\rho_1$ and $\rho_2$ are the densities of rubber ($\rho_1$ = 0.91 g/cm$^3$) and toluene ($\rho_2$ = 0.865 g/cm$^3$), respectively; $\varphi_r$ is the volume fraction of the swollen rubber; $V_0$ is the molar volume of toluene (106.2 cm$^3$/mol); $n$ is the number of active network chain segments per unit volume (crosslinking density); and $\chi$ is the Flory–Huggins polymer–solvent interaction term, which is 0.430 for toluene [35].

### 2.6. Differential scanning calorimetry (DSC) measurements

DSC measurements were performed using a DSC Q20 calorimeter (TA Instruments, USA) under a $N_2$ atmosphere. Temperature and enthalpy were calibrated using an indium standard. Samples with a mass of 5–8 mg were maintained at 100 °C for 3 min to eliminate their thermal histories, following which they were cooled to –50 °C at a rate of 10 °C·min$^{-1}$. The samples were subsequently heated to 100 °C at a rate of 10 °C·min$^{-1}$. The cooled and subsequently heated traces were recorded for analysis. The degree of crystallinity ($X_c$) for each portion of the sample was calculated using the Equation (3):

$$X_c=\frac{\Delta H_m}{\Delta H_m^*}\cdot 100\% \quad (3)$$

where $\Delta H_m$ and $\Delta H_m^*$ are the melting enthalpy and ideal melting enthalpy of a certain polymer portion (approximately 186.8 J·g$^{-1}$ for EUR [32, 36]), respectively.

### 2.7. Shape-memory property analysis

Dynamic mechanical analyses were carried out using a Q800 Dynamical Mechanical Analyzer (DMA) (TA Instruments, USA) in the 'Controlled Force' mode. The preload was 0.001 N, and the frequency was 1 Hz. Test samples were cut into rectangles,

with a width of 4.0 mm, a thickness of 1.0 mm, and a length of 30.0 mm. The initial clamp gap was set to 6.0–8.0 mm. The heating and cooling rates were both 5 °C·min$^{-1}$.

To begin with, all samples were maintained isothermally at 100 °C for 3 min to melt the crystalline domain completely. The initial strain was denoted as $\varepsilon_0$. A load of 3 N was then applied at a speed of 0.3 N·min$^{-1}$, and the sample was cooled to –50 °C at a rate of 5 °C·min$^{-1}$ for the crystalline domains to freeze completely ($\varepsilon_{1,load}$). The load was then removed ($\varepsilon_1$). Finally, the sample was reheated to 100 °C at a rate of 5 °C·min$^{-1}$ and maintained isothermally for 15 min ($\varepsilon_{0,rec}$).

The shape fixity ($R_f$) and shape recovery ($R_r$) ratios are crucial parameters in shape-memory characterization. The two properties can be quantified as shown by Equations (4) and (5):

$$R_f(0 \rightarrow 1) = \frac{\varepsilon_1 - \varepsilon_0}{\varepsilon_{1,load} - \varepsilon_0} \cdot 100\% \quad (4)$$

$$R_r(1 \rightarrow 0) = \frac{\varepsilon_1 - \varepsilon_{0,rec}}{\varepsilon_1 - \varepsilon_0} \cdot 100\% \quad (5)$$

### 2.8. Scanning electron microscopy (SEM)

Sample sections of EUR composites were first fractured in liquid nitrogen. They were then placed on a double-sided sticky carbon tape mounted on a copper sample holder coated with platinum for SEM analysis. The fracture appearances of the sample sections were observed using a JEOL JSM-6700 field-emission SEM instrument.

## 3. Results and discussion

### 3.1. Cure characteristics of EUR composites

Figure 2 shows the variation in the cure characteristics of EUR composites with the variation in the CCB content, where $M_H$ and $M_L$ represent the maximum and minimum torque values, respectively, during the molding of the samples. While there was a gradual increase in $M_H$ with the addition of CCB (Figure 2a), there was only a small increase in $M_L$; that is, it increased only slightly with the increase in the CCB content. Thus, $M_H - M_L$ showed an increasing trend, implying the increase in the crosslinking rate in composites. We also measured the crosslinking density of the composites using the swelling method shown in Figure 3. The results showed that the crosslinking density of the composites increased with the increase in the CCB content, which was consistent with the results of $M_H - M_L$. In Figure 2b,

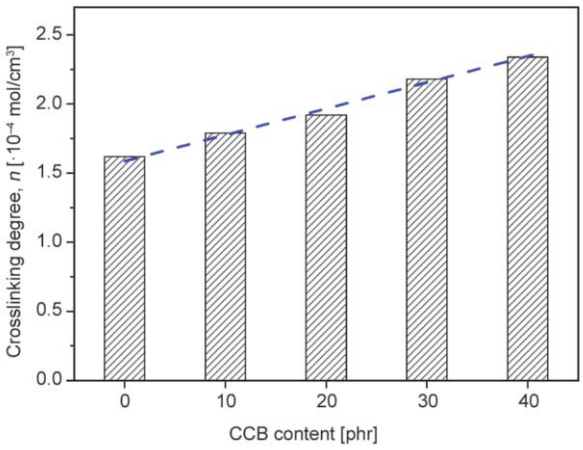


**Figure 3.** Crosslinking density of EUR composites with different CCB content.

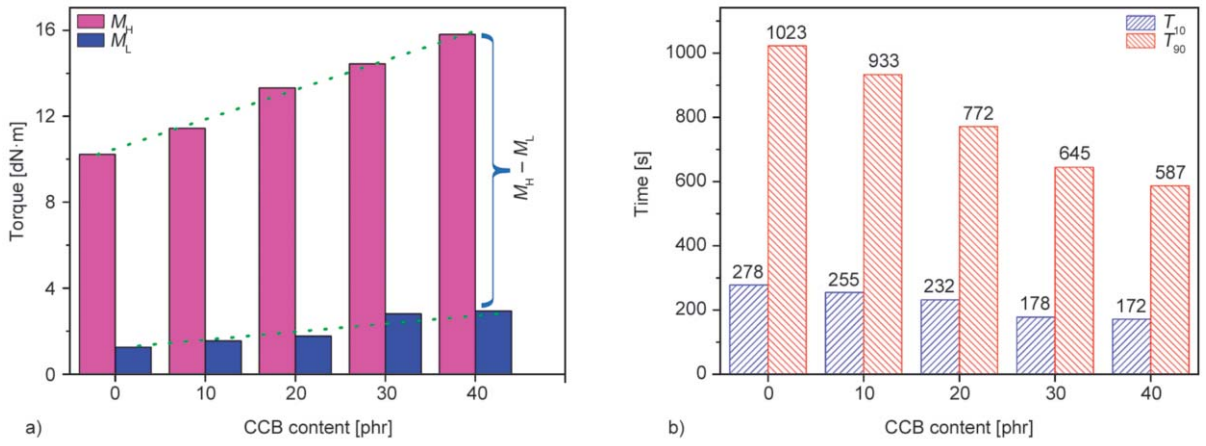


**Figure 2.** Effect of CCB content on the cure characteristics of EUR composites: (a) maximum torque ($M_H$) and minimum torque ($M_L$) during the molding process, and (b) the scorch time ($T_{10}$) and the curing time ($T_{90}$).

$T_{10}$ represents the scorch time, which is usually defined as the time for samples' torque added 10 units during the molding process. $T_{90}$ represents the time for samples' torque added 90 units during the molding process, which is closely linked with optimum cure time. $T_{10}$ and $T_{90}$ showed a downward trend with the increase of CCB content. The result indicated that the addition of CCB could shorten the curing time of the composites ($T_{90}$). However, the short scorch time poses a challenge for the safe processing of rubber composites.

### 3.2. Mechanical properties of EUR composites

The effect of CCB content on the mechanical properties of the EUR composites is shown in Figure 4. The tensile strength of the composites was observed to increase from 20.4 to 25.8 MPa when the composites were filled with 10 phr CCB, proving the obvious reinforcement effect of CCB. The tensile strength was found to decrease slightly from 25.8 to 23.2 MPa when the CCB content was increased from 10 to 40 phr. However, the modulus at 100% elongation increased from 7.2 to 12.7 MPa with the increase in the CCB content. The hardness of the composites was observed to increase, and the elongation at break was observed to decrease with the increase in the CCB content (Figure 4b). This phenomenon showed that the addition of CCB worsened the plasticity of the composites.

### 3.3. DSC analysis

Carbon black, as the major reinforcement filler, was found to have an obvious reinforcement effect in natural rubber. However, the reinforcement effect in EUR was obvious when the CCB content was 10 phr, with the tensile strength of the EUR composites decreasing slightly when the CCB content was 20–40 phr. Therefore, DSC was used to characterize the crystalline properties of the composites and explore the reason for this phenomenon. EUR crystallizes easily due to its regular trans-structure of the macromolecular chains. The addition of CCB is believed to affect the mechanical and thermal properties of the composites. The crystalline portions in EUR composites play an important role in the shape-memory behavior of composites, which act as the reversible phase during the shape-memory process. Therefore, it is critical to investigate the effect of CCB content on the crystallization of the composites. Both the thermal properties and the transition temperatures of the shape-memory composites were measured using DSC (Figure 5). The degree of crystallinity and the melting range were obtained from the resulting DSC curves. The crystallinity of the composites decreased from 20.13 to 18.47% with the increase in the CCB content (Table 2). This phenomenon may be attributed to the crystalline zone of EUR in the composites getting destroyed due to the addition of CCB. Furthermore, the melting temperature changed slightly with the increase in the CCB content.

**Table 2.** The thermal properties of EUR composites.

| Properties | | EUR/CCB composites | | | |
|---|---|---|---|---|---|
| | | A | B | C | D |
| $X_c$ | [%] | 20.13 | 19.75 | 19.47 | 18.47 |
| $\Delta H_m$ | [J/g] | 34.18 | 28.75 | 27.97 | 26.35 |
| $T_c$ | [°C] | 14.50 | 15.10 | 17.50 | 20.50 |
| $T_m$ | [°C] | 43.3, 52.2 | 43.5, 52.3 | 43.3, 52.2 | 43.5, 52.3 |

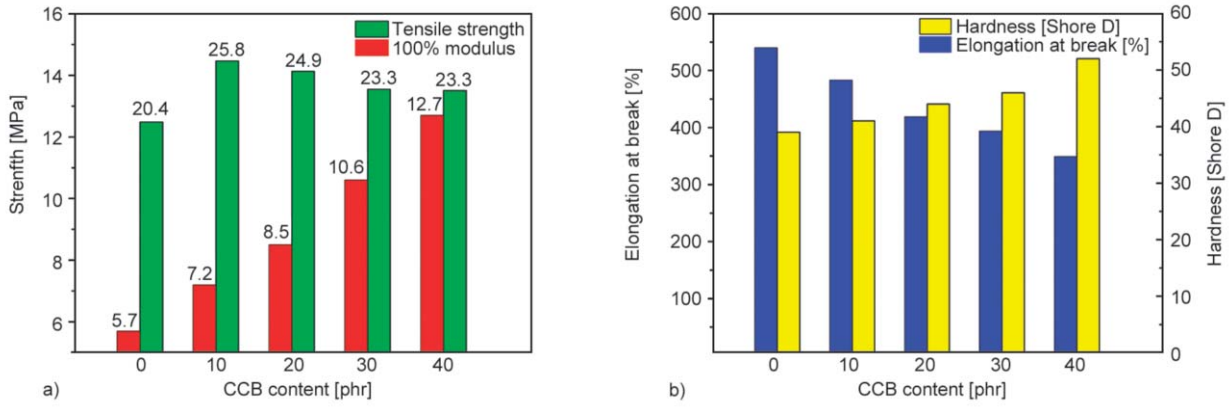


**Figure 4.** Effect of CCB dosage on the mechanical properties of the EUR composites: (a) tensile strength and 100% modulus, (b) hardness and elongation at break.

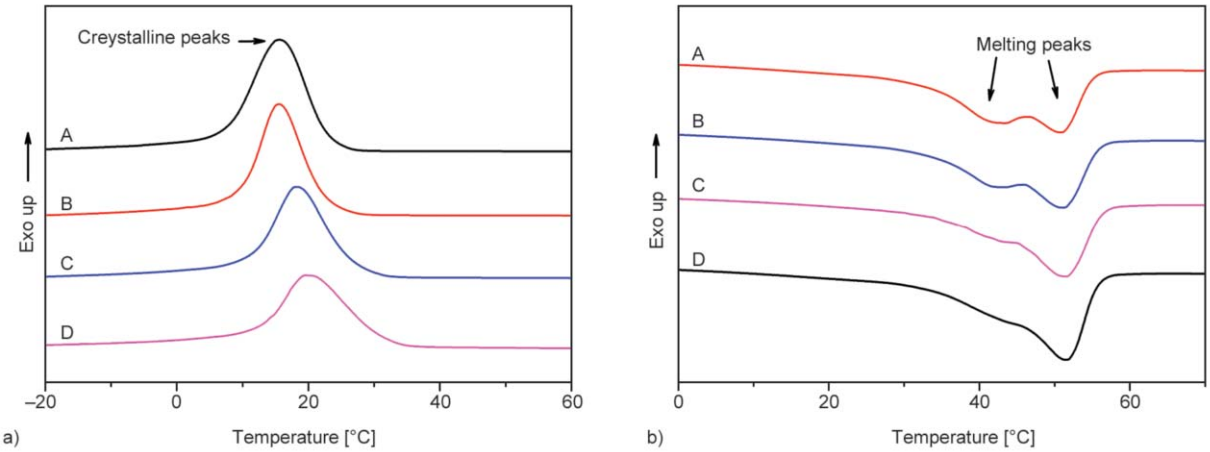


**Figure 5.** DSC curves of EUR composites with different CCB content (a) cooling scan and (b) heating scan.

### 3.4. Shape-memory analysis

The shape-memory properties of EUR composites were then measured using a dynamic mechanical analyzer (Figure 6 and Table 3). The SMP specimens were maintained isothermally above the Ttrans (100 °C). The crystalline regions of EUR, when melted, acted as reversible domains in the composites. Meanwhile, the crosslinking network acted as the fixed domain, restricting the plastic slippage of the molecular chains. We found that the shape fixity ratio ($R_f$) decreased from 90.4 to 83.3%, and the shape recovery ratio ($R_r$) of the composites increased from 91.5 to 97.1%, with the increase in the CCB content. The decrease in $R_f$ was due to the decrease in the crystal portions as the reversible phase in the EUR composite; the observation was consistent with the thermal properties revealed by DSC tests. The increase in $R_r$ was attributed to the strengthening effect of the crosslinking network as the fixed phase in the composites. There was not only the crosslinking network of polymer chains but also the network of the CCBs as the filler. Thus, $R_f$ and $R_r$ showed different tendencies with the addition of CCB.

### 3.5. Electronic shape-memory analysis

We investigated the electro-induced shape-memory properties of EUR composites (Figure 7). The course of these experiments may be summed up as follows:

**Table 3.** The shape memory properties of the EUR/CCB composites.

| Properties | EUR/CCB composites | | | |
|---|---|---|---|---|
| | A | B | C | D |
| $R_f$ [%] | 90.4±0.3 | 89.3±0.4 | 85.8±0.5 | 83.3±0.4 |
| $R_r$ [%] | 91.5±0.3 | 92.0±0.3 | 94.3±0.4 | 97.1±0.4 |

First, we gave the sample a temporary 'V' shape by heating and cooling the strip-shaped sample. After the 'V'-shaped sample was electrified, we observed the recovery process of electro-induced shape-memory materials in real-time. The experiments were carried out using composites at a voltage of 80 V and a CCB concentration of 40 phr. We found that the materials gradually returned to the original shape (linear) when the electrification time changed from 5, 10, 15, to 30 s. We fixed the temporary 'V' shape with an angle of 10~15°. With the increase in time, the temporary angle changed to ~40° at 10 s, ~62° at 15 s, ~113° at 20 s, and ~131° at 25 s. At 30 s, the angle completely restored to 180°. Thus, it took only 30 s for the composite to completely return to its original shape. From the above experiment, we observed that the recovery deformation rate of composites changed from slow to fast. Therefore, we thought that when the electricity was first turned on, the composites first absorbed the heat and thus restored their shape by heating.

Thus far, we have described the electro-induced shape-memory behavior of EUR composites. However, whether there is an effect of voltage on the electro-induced shape-memory composites remains to be uncovered. Therefore, we stimulated EUR composites at different voltage values. We observed that the larger the amount of CCBs that was added to the composites, the easier it was to recover them to their original shape under conditions of low voltage. As shown in Table 4, when the CCB content was 40 phr, the composites were restored to their initial morphology at a voltage of 120 V in 10 s. The higher the voltage, the faster was the recovery speed. Composites without

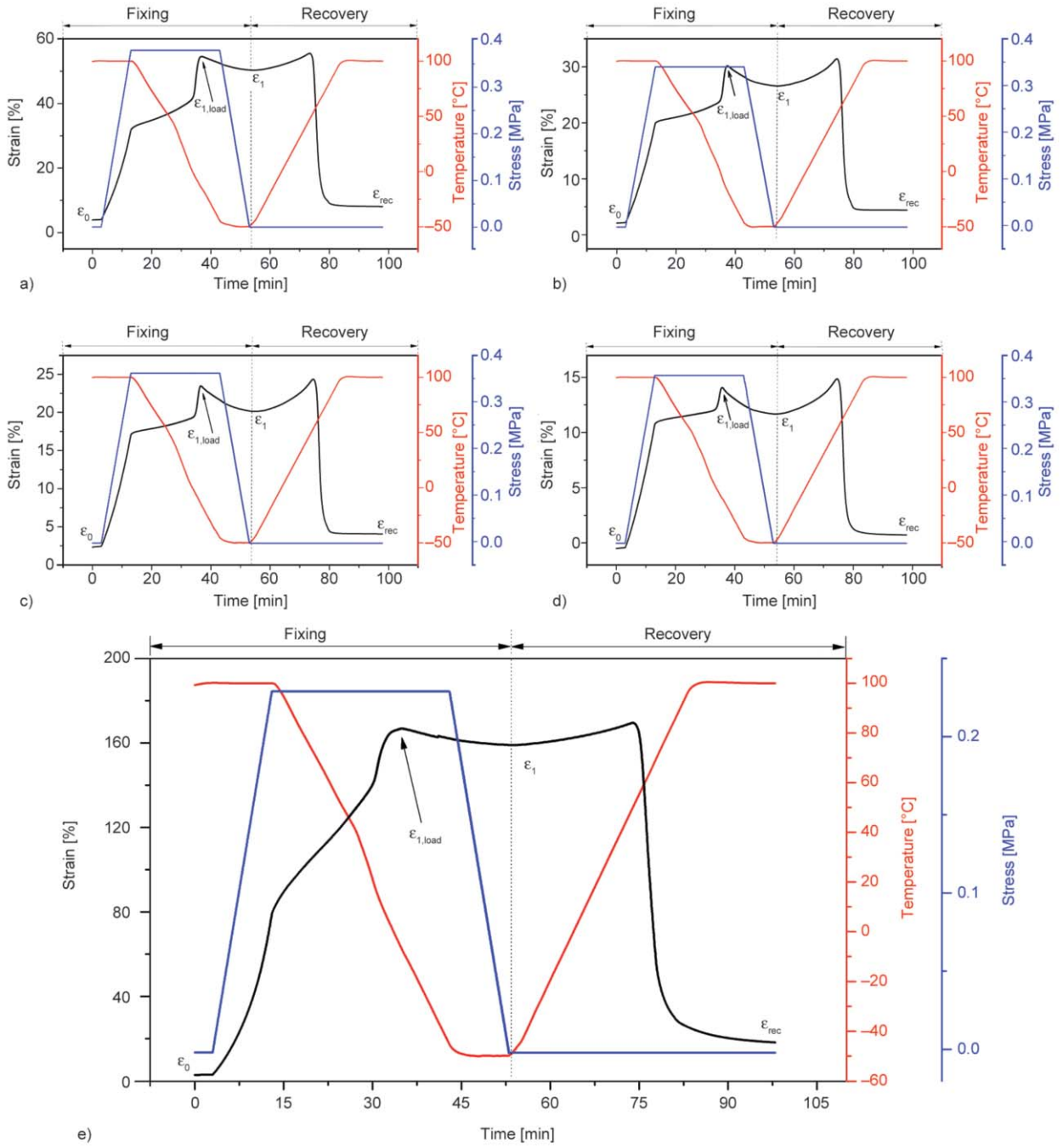


**Figure 6.** Shape memory properties of EUR composites with different CCB content (a) 10 phr, (b) 20 phr, (c) 30 phr, (d) 40 phr, (e) 0 phr.

**Table 4.** The recovery time in voltage- triggered shape memory behavior of EUR composites.

| Properties | Recovery time in voltage-triggered shape memory behavior | | | |
|---|---|---|---|---|
| | A | B | C | D |
| **CCB content** | **10** | **20** | **30** | **40** |
| 60 V | – | – | – | 150 s |
| 80 V | – | – | 100 s | 80 s |
| 100 V | – | – | 60 s | 30 s |
| 120 V | – | – | 25 s | 10 s |

CCB did not display any electro-induced shape-memory performance.

### 3.6. Dispersion and conductivity properties of the composites

Composites filled with conductive fillers are heterogeneous dispersion systems. Currently, there are two main theories that explain the conductive mechanism of composites. First, the conductive path theory, according to which the conductive particles are

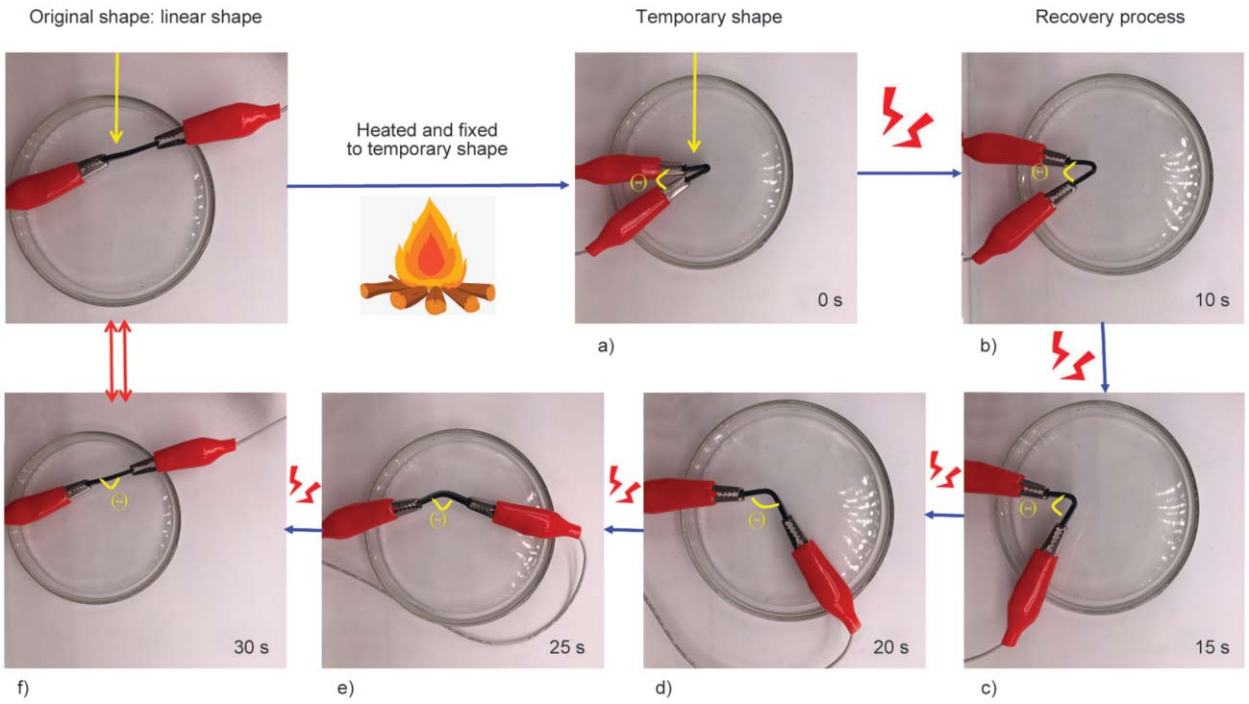


**Figure 7.** The real-time shape recovery process under electrification (a) 0 s, (b) 10 s, (c) 15 s, (d) 20 s, (e) 25 s, (f) 30 s.

interconnected, and the electrons generate the conductive phenomenon by overlapping conductors. Second, the tunnel conductive effect theory, according to which the electrons can also migrate in the gap between the conductive particles, resulting in the conductive phenomenon. In order to investigate the conductive mechanism of these composites, SEM was employed, and the dispersion of CCB in the composites was observed (Figure 8). We found that most of the CCB existed as separate particles and were not in contact with each other or even in partial contact when the content of CCB was low. With the increase in the dosage of CCB, an overlap phenomenon was expected between the CCB particles, resulting in a relatively complete conductive path.

The ESMPs usually possess excellent conductivity. Therefore, it is necessary to evaluate the conductivity of materials by measuring their resistivity. The volume resistivity of EUR composites with different CCB contents is shown in Figure 9. The fitted curve was smooth and continuous. We found that the volume resistivity of the EUR composites changed dramatically with the addition of CCB, indicating the seepage transition of materials from an insulator to a conductor and the formation of the conductive pathway through the composites with the introduction of the CCB filler. When the amount of CCB exceeded 20 phr, a relatively perfect conductive path was formed, and the volume resistivity was relatively stable in the composites. During this process, the resistance heat generated by the addition of conductive CCBs led to the increase in the temperature to $T_{trans}$, thus restoring the composites to their original shape.

### 3.7. Schematic diagram

A schematic diagram was proposed for further comprehension of the shape-memory behavior of EUR/CCB composites. As shown in Figure 10, the blue color represents the EUR molecular chains. Disorderedly dispersed lines in the composites represent the amorphous chain segments and the regularly arranged lines in the crystalline regions. Dark blue dots, distributed among the molecular chains, represent aggregations of CCB. Orange spots represent the crosslinking points in the composites. When the sample temperature was maintained isothermally at 100 °C, all of the crystalline regions melted. During mechanical loading and cooling, a temporary shape was formed and fixed. After load removal and reheating, the specimens could return to their original shapes. The schematic reflects the softening, deforming, fixing, and restoring of the crystalline parts in the composites during the heating and electrification processes.

During the response to the electrical stimulation, a certain amount of CCB was found to form a conductive path in the composites. When the electrical energy is transformed into heat energy, the crystallization

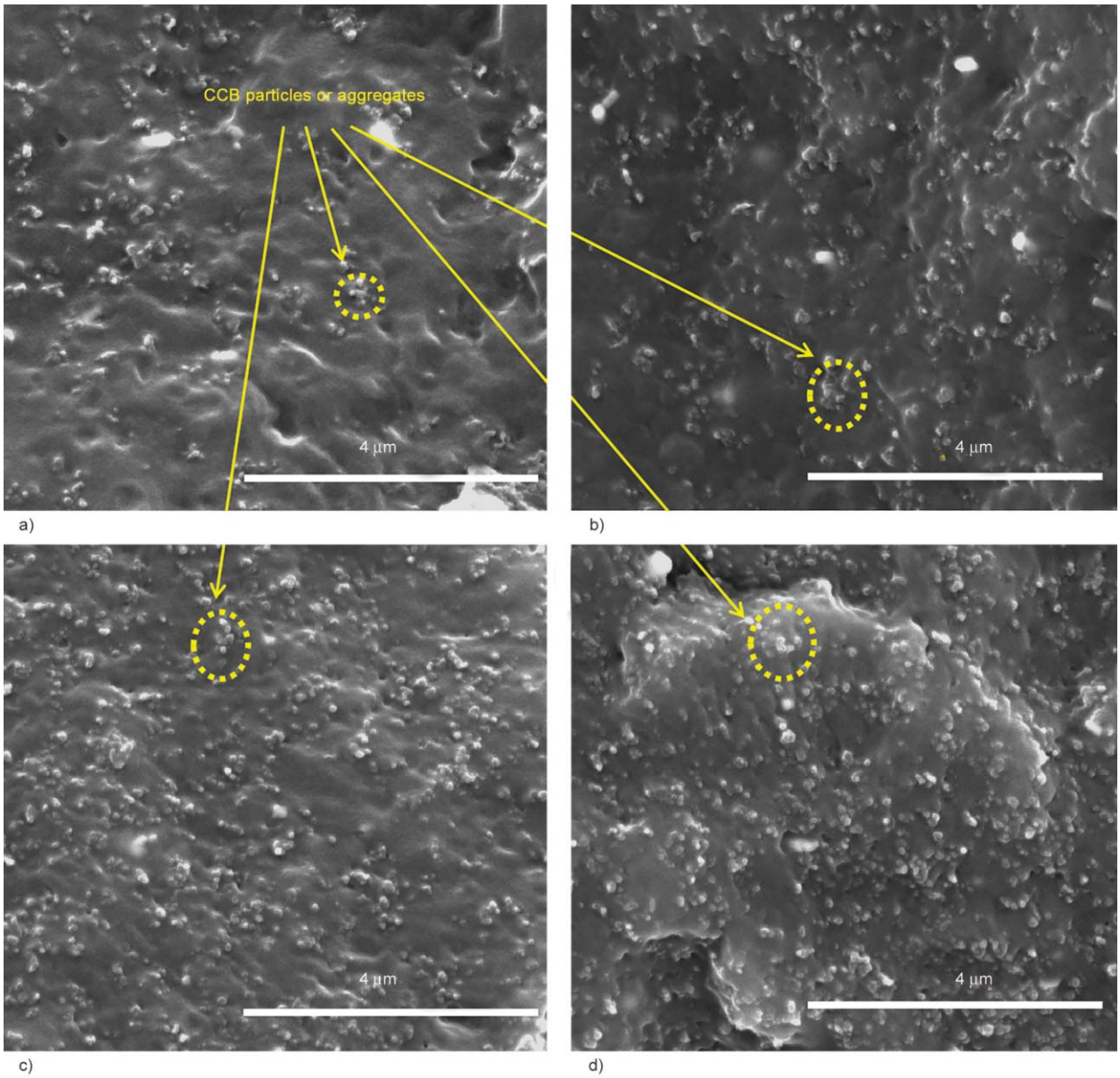


**Figure 8.** SEM images of EUR composites with different CCB content (a) 10 phr, (b) 20 phr, (c) 30 phr, (d) 40 phr.

zone inside the composite material can be melted, which provides sufficient conditions for the deformation of the composites. In this case, the composites can be deformed under external force. After removing the power supply and maintaining the external force, the temporary shape of composites can be fixed. When the composites are electrified again, the crystalline zones of the composites can be melted again, and the crosslinked network structure in the composite will drive the composites to return to their original shape. The composites will complete the shape-memory behavior in response to the electrical stimulation.

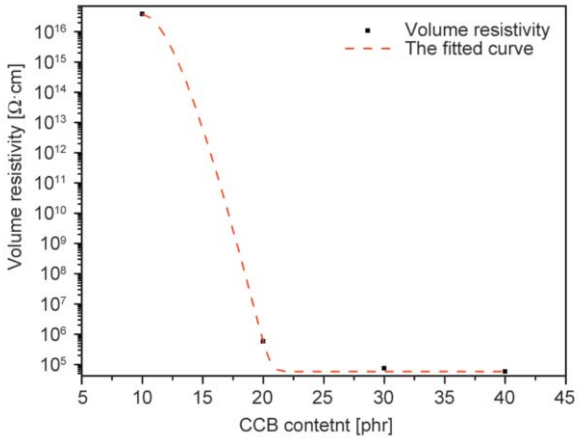


**Figure 9.** The volume resistivity of EUG composites with different CCB content.

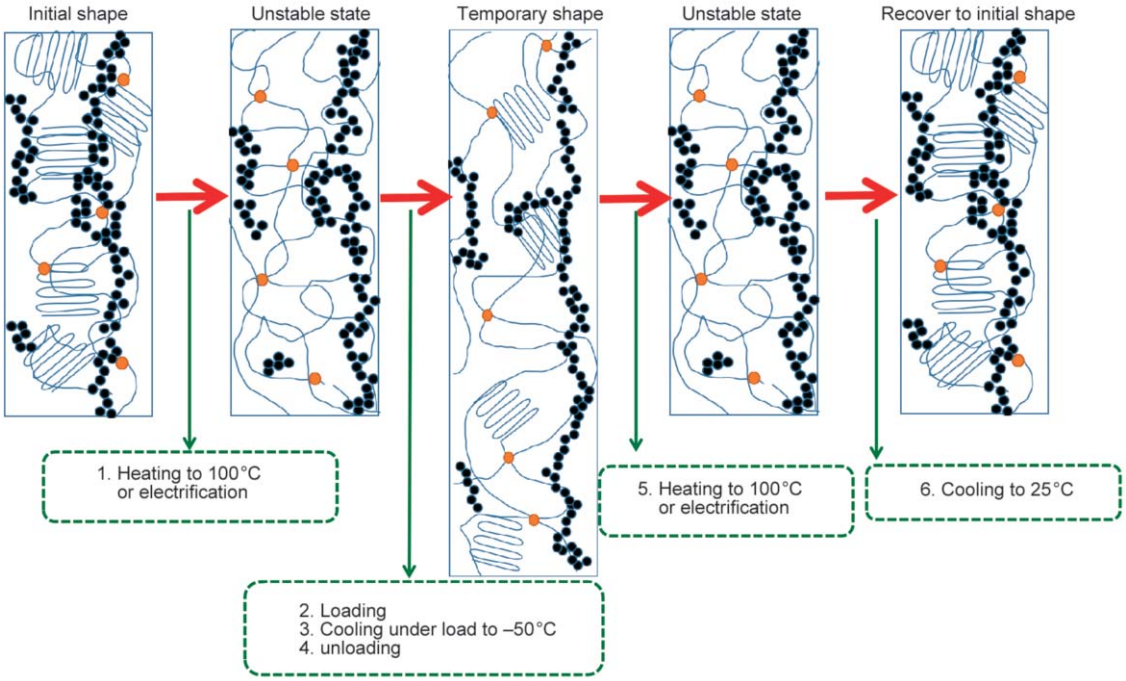


**Figure 10.** Schematic diagram of EUR/CCB composites in the shape memory process.

## 4. Conclusions

In this study, we prepared thermo- and electro-induced double-stimulus shape-memory composites comprising natural EUR and CCBs, and demonstrated their excellent properties. The addition of functional filler CCBs could endow the electro-induced and voltage-triggered shape-memory properties of composites. We believe that our findings have provided an insightful understanding of the dual shape-memory behavior of EUR composites.

## Acknowledgements

Financial support from the National Natural Science Foundation of China (grant No. 51303092, 51573194), Major scientific and technological innovation projects in Shandong Province, China [2019JZZY020223] and the Shandong natural science funds [ZR2019MEM016, ZR2019MEM028] is gratefully acknowledged.

## References

[1] Lendlein A., Kelch S.: Shape-memory polymers. Angewandte Chemie, **41**, 2034–2057 (2002). https://doi.org/10.1002/1521-3773(20020617)41:12<2034::AID-ANIE2034>3.0.CO;2-M

[2] Lendlein A.: Progress in actively moving polymers. Journal of Materials Chemistry, **20**, 3332–3334 (2010). https://doi.org/10.1039/C004361N

[3] Kang S. M., Lee S. J., Kim B. K.: Shape memory polyurethane foams. Express Polymer Letters, **6**, 63–69 (2012). https://doi.org/10.3144/expresspolymlett.2012.7

[4] Chow W. S., Mohd Ishak Z. A.: Smart polymer nanocomposites: A review. Express Polymer Letters, **14**, 416–435 (2020). https://doi.org/10.3144/expresspolymlett.2020.35

[5] Garle A., Kong S., Ojha U., Budhlall B. M.: Thermoresponsive semicrystalline poly(ε-caprolactone) networks: Exploiting cross-linking with cinnamoyl moieties to design polymers with tunable shape memory. ACS Applied Materials and Interfaces, **4**, 645–657 (2012). https://doi.org/10.1021/am2011542

[6] Guo W., Kang H., Chen Y., Guo B., Zhang L.: Stronger and faster degradable biobased poly(propylene sebacate) as shape memory polymer by incorporating boehmite nanoplatelets. ACS Applied Materials and Interfaces, **4**, 4006–4014 (2012). https://doi.org/10.1021/am300828u

[7] Fan M-M., Yu Z-J., Luo H-Y., Zhang S., Li B-J.: Supramolecular network based on the self-assembly of γ-cyclodextrin with poly(ethylene glycol) and its shape memory effect. Macromolecular Rapid Communications, **30**, 897–903 (2009). https://doi.org/10.1002/marc.200800712

[8] Zheng X., Zhou S., Li X., Weng J.: Shape memory properties of poly(D,L-lactide)/hydroxyapatite composites. Biomaterials, **27**, 4288–4295 (2006). https://doi.org/10.1016/j.biomaterials.2006.03.043

[9] Lendlein A., Jiang H., Jünger O., Langer R.: Light-induced shape-memory polymers. Nature, **434**, 879–882 (2005). https://doi.org/10.1038/nature03496

[10] Mayer G., Heckel A.: Biologically active molecules with a 'light switch'. Angewandte Chemie-International Edition, **45**, 4900–4921 (2006). https://doi.org/10.1002/anie.200600387

[11] Wu L., Jin C., Sun X.: Synthesis, properties, and light-induced shape memory effect of multiblock polyester-urethanes containing biodegradable segments and pendant cinnamamide groups. Biomacromolecules, **12**, 235–241 (2011). https://doi.org/10.1021/bm1012162

[12] Meng H., Li G.: A review of stimuli-responsive shape memory polymer composites. Polymer, **54**, 2199–2221 (2013). https://doi.org/10.1016/j.polymer.2013.02.023

[13] Ma X., Tian H.: Stimuli-responsive supramolecular polymers in aqueous solution. Accounts of Chemical Research, **47**, 1971–1981 (2014). https://doi.org/10.1021/ar500033n

[14] Yakacki C. M., Shandas R., Lanning C., Rech B., Eckstein A., Gall K.: Unconstrained recovery characterization of shape-memory polymer networks for cardiovascular applications. Biomaterials, **28**, 2255–2263 (2007). https://doi.org/10.1016/j.biomaterials.2007.01.030

[15] Lendlein A., Langer R.: Biodegradable, elastic shape-memory polymers for potential biomedical applications. Science, **296**, 1673–1676 (2002). https://doi.org/10.1126/science.1066102

[16] El Feninat F., Laroche G., Fiset M., Mantovani D.: Shape memory materials for biomedical applications. Advanced Engineering Materials, **4**, 91–104 (2002). https://doi.org/10.1002/1527-2648(200203)4:3<91::AID-ADEM91>3.0.CO;2-B

[17] Liu X., Zhao K., Gong T., Song J., Bao C., Luo E., Weng J., Zhou S.: Delivery of growth factors using a smart porous nanocomposite scaffold to repair a mandibular bone defect. Biomacromolecules, **15**, 1019–1030 (2014). https://doi.org/10.1021/bm401911p

[18] Yu X., Wang L., Huang M., Gong T., Li W., Cao Y., Ji D., Wang P., Wang J., Zhou S.: A shape-memory stent of poly(ε-caprolactone-*co*-DL-lactide) copolymer for potential treatment of esophageal stenosis. Journal of Materials Science: Materials in Medicine, **23**, 581–589 (2012). https://doi.org/10.1007/s10856-011-4475-4

[19] Zhou J., Li H., Liu W., Dugnani R., Tian R., Xue W., Chen Y., Guo Y., Duan H., Liu H.: A facile method to fabricate polyurethane based graphene foams/epoxy/carbon nanotubes composite for electro-active shape memory application. Composites Part A: Applied Science and Manufacturing, **91**, 292–300 (2016). https://doi.org/10.1016/j.compositesa.2016.10.021

[20] Hassanzadeh-Aghdam M. K., Ansari R.: Thermal conductivity of shape memory polymer nanocomposites containing carbon nanotubes: A micromechanical approach. Composites Part B: Engineering, **162**, 167–177 (2019). https://doi.org/10.1016/j.compositesb.2018.11.003

[21] Shi Y., Chen Z.: Function-driven design of stimuli-responsive polymer composites: Recent progress and challenges. Journal of Materials Chemistry C, **6**, 11817–11834 (2018). https://doi.org/10.1039/C8TC02980F

[22] Koerner H., Price G., Pearce N. A., Alexander M., Vaia R. A.: Remotely actuated polymer nanocomposites–stress-recovery of carbon-nanotube-filled thermoplastic elastomers. Nature Materials, **3**, 115–120 (2004). https://doi.org/10.1038/nmat1059

[23] Leng J., Lan X., Liu Y., Du S.: Shape-memory polymers and their composites: Stimulus methods and applications. Progress in Materials Science, **56**, 1077–1135 (2011). https://doi.org/10.1016/j.pmatsci.2011.03.001

[24] Qi X., Dong P., Liu Z., Liu T., Fu Q.: Selective localization of multi-walled carbon nanotubes in bi-component biodegradable polyester blend for rapid electroactive shape memory performance. Composites Science and Technology, **125**, 38–46 (2016). https://doi.org/10.1016/j.compscitech.2016.01.023

[25] Du F-P., Ye E-Z., Yang W., Shen T-H., Tang C-Y., Xie X-L., Zhou X-P., Law W-C.: Electroactive shape memory polymer based on optimized multi-walled carbon nanotubes/polyvinyl alcohol nanocomposites. Composites Part B: Engineering, **68**, 170–175 (2015). https://doi.org/10.1016/j.compositesb.2014.08.043

[26] Ma L., Zhao J., Wang X., Chen M., Liang Y., Wang Z., Yu Z., Hedden R. C.: Effects of carbon black nanoparticles on two-way reversible shape memory in cross-linked polyethylene. Polymer, **56**, 490–497 (2015). https://doi.org/10.1016/j.polymer.2014.11.036

[27] Qi X., Xiu H., Wei Y., Zhou Y., Guo Y., Hang R., Bai H., Fu Q.: Enhanced shape memory property of polylactide/thermoplastic poly(ether)urethane composites *via* carbon black self-networking induced *co*-continuous structure. Composites Science and Technology, **139**, 8–16 (2017). https://doi.org/10.1016/j.compscitech.2016.12.007

[28] Lan X., Liu Y., Lv H., Wang X., Leng J., Du S.: Fiber reinforced shape-memory polymer composite and its application in a deployable hinge. Smart Materials and Structures, **18**, 024002/1–024002/6 (2009). https://doi.org/10.1088/0964-1726/18/2/024002

[29] Kim H., Abdala A. A., Macosko C. W.: Graphene/polymer nanocomposites. Macromolecules, **43**, 6515–6530 (2010). https://doi.org/10.1021/ma100572e

[30] Liu X., Li H., Zeng Q., Zhang Y., Kang H., Duan H., Guo Y., Liu H.: Electro-active shape memory composites enhanced by flexible carbon nanotube/graphene aerogels. Journal of Materials Chemistry A, **3**, 11641–11649 (2015). https://doi.org/10.1039/C5TA02490K

[31] Xia L., Chen S., Fu W., Qiu G.: Shape memory behavior of natural *Eucommia ulmoides* gum and low-density polyethylene blends with two response temperatures. Polymers, **11**, 580/1–580/11 (2019). https://doi.org/10.3390/polym11040580

[32] Xia L., Zhang M., Gao H., Qiu G., Xin Z., Fu W.: Thermal- and water-induced shape memory *Eucommia ulmoides* rubber and microcrystalline cellulose composites. Polymer Testing, **77**, 105910/1–105910/8 (2019). https://doi.org/10.1016/j.polymertesting.2019.105910

[33] Xia L., Wang Y., Lu N., Xin Z.: Facile fabrication of shape memory composites from natural *Eucommia* rubber and high density polyethylene. Polymer International, **66**, 653–658 (2017). https://doi.org/10.1002/pi.5291

[34] Arroyo M., López-Manchado M. A., Herrero B.: Organo-montmorillonite as substitute of carbon black in natural rubber compounds. Polymer, **44**, 2447–2453 (2003). https://doi.org/10.1016/S0032-3861(03)00090-9

[35] Zhang J., Xue Z.: A comparative study on the properties of *Eucommia ulmoides* gum and synthetic trans-1,4-polyisoprene. Polymer Testing, **30**, 753–759 (2011). https://doi.org/10.1016/j.polymertesting.2011.06.010

[36] Xia L., Chen S., Fu W., Qiu G.: Shape memory behavior of natural *Eucommia ulmoides* gum and low-density polyethylene blends with two response temperatures. Polymers, **11**, 580/1–580/11 (2019). https://doi.org/10.3390/polym11040580